NUMERICAL SIMULATION OF JANUARY 28 COLD AIR OUTBREAK DURING *GALE* PART II: THE MESOSCALE CIRCULATION AND MARINE BOUNDARY LAYER

CHING-YUANG HUANG and SETHU RAMAN

Department of Marine, Earth and Atmospheric Sciences, North Carolina State University, Raleigh, NC 27695-8208, U.S.A.

(Received in final form 18 December, 1990)

Abstract. A two-dimensional (2-D) mesoscale numerical model is applied to simulate the January 28 cold-air outbreak over the Gulf Stream region during the Intensive Observation Period-2 (IOP-2) of the 1986 Genesis of Atlantic Lows Experiment (GALE). The model utilizes a turbulence closure which involves the turbulent kinetic energy (TKE) and dissipation (ϵ) equations and combines the level 2.5 formulations of Mellor and Yamada (1982) for better determination of the eddy Prandtl number.

The modeled marine boundary layer (MBL) is in good agreement with the observations (Wayland and Raman, 1989) showing a low-level jet west of the Gulf Stream warm core and a constrained boundary layer due to the middle-level (2–4.5 km) stable layer. The MBL-induced single cloud and rain band first appears east of the Gulf Stream boundary, and then moves offshore at the speed of the circulation front. The front, however, moves slightly slower than the ambient flow. Removal of the tropopause does not influence the low-level circulation and the movement of the front. The speed of the front is slightly larger in the baroclinic downshear flow than in the barotropic flow. The results also indicate that the observed high cloud streets propagating downwind of the Gulf Stream may be related to upper-level baroclinic lee waves triggered by an elevated density mountain. The density mountain waves, however, become evanescent as the baroclinity (which gives a larger Scorer parameter) is removed.

The modeled 2-D circulation systems are found to be sensitive to differing eddy Prandtl numbers, in contrast to the 1-D model results presented in Part I. Sensitivities become increasingly important as the clouds begin to interact with the MBL. A constant eddy Prandtl number of unity produces a more slantwise convection compared to that by the level 2.5 case. Cloud development is stronger in slantwise convection than in upright convection. The fastest development of clouds can be explained in terms of the conditional symmetric instability (CSI), which begins as the MBL baroclinity becomes sufficiently large.

1. Introduction

In Part I (Huang and Raman, 1991), we mentioned the importance of Gulf Stream warming in facilitating Atlantic cyclogeneses during winter. To understand the effects of the lower boundary conditions, we first performed sensitivity tests of different turbulence closure schemes, since turbulent transfer in the planetary boundary layer (PBL) is the primary mechanism responsible for energy transport from the ocean into the atmosphere. A successful mesoscale simulation of air mass modification over an oceanic region would to a large extent depend on the turbulence closure used.

A potential turbulence closure scheme examined in Part I is the modified E-ϵ

Boundary-Layer Meteorology **56**: 51–81, 1991.

closure which contains some advantageous features of the level 2.5 one, proposed by Mellor and Yamada (1974, 1982). The original E-ϵ closure relies on two prognostic equations, one for turbulent kinetic energy (TKE) and the other for turbulent dissipation (ϵ). An assumption of mixing-length scales using formulations such as Blackadar's is not required if the turbulent dissipation equation is used with Kolmogorov's hypothesis for eddy mixing length, $l \sim E^{3/2}/\epsilon$. The ratio between eddy diffusivities (K) for momentum and heat, i.e., the eddy Prandtl number (K_M/K_θ), which is assumed constant in conventional E-ϵ closure schemes can be better determined using the level 2.5 formulation based on $K \sim l\, E^{1/2}$ (for details, see Part I). When applied to 1-D PBL flows under various stability conditions, this modified E-ϵ closure model, however, did not give significantly better results as compared to the simplest E-model which involves only the TKE equation. Indeed, little sensitivity of the results in the 1-D flow tests was caused by different assumptions for the TKE closure because of the existence of a global similarity that reduces the importance of increased freedom of the closures. The 1-D model results were also found to be similar for Blackadar's and Kolmogorov's formulations although there were large differences between the eddy mixing lengths. Effects of excessively large mixing length on eddy diffusivity were offset by decreased turbulence intensity. Hence, the 1-D model tests did not show the important role of the eddy Prandtl number.

The results for 1-D flow can not be extended to 2-D flow since advection effects can play an important role in changing the PBL structure by laterally redistributing the energies of the mean flow (in grid scale) and the turbulence (in subgrid scale). A number of simple or more advanced turbulence closure models were successful in simulations of 1-D PBLs of the type-Wangara Day 33–34 (e.g., Yamada and Mellor, 1975; Sun and Ogura, 1980; Mailhot and Benoit, 1982). Better agreement between the model results and the observations usually occurs for convective conditions since advection effects may be less important. However, important lateral variations of convective flow may be caused by large horizontal differentials that may also exist in the lower boundary. The sea breeze front is an example where nonlinear advection is strong enough to change the system from Benard convection with pure vertical diffusion to a mesoscale circulation. Advection also affects the structure of the marine boundary layer (MBL) over the oceanic baroclinic zone.

A goal of this study is to understand the response of the MBL as cold air advects over a warm oceanic baroclinic zone using the mesoscale numerical model described in Part I. One such event observed during GALE (1986) was the January 28 IOP-2 (Intensive Observation Period II) when an extremely cold dry air mass moved offshore from a north-westerly direction, passed the Atlantic coast and then the Gulf Stream region. The cold air outbreak is a severe weather phenomenon that occurs over the east coast during winter. A continental cold air mass can be significantly changed as it moves offshore. This air-sea interaction process is believed to moisten and pre-condition the atmosphere for possible cyclogenesis or frontogenesis. A 2-D model would help to determine the degree of air mass

modification and the induced low-level circulations in undisturbed ambient conditions (Huang and Raman, 1990a).

2. Initial Conditions and Model Domain

Detailed analysis of the synoptic conditions on 28 January 1986 were given by Uccellini *et al.* (1986) and a summary of these conditions was shown in Figure 3 of Wayland and Raman (1989). At 0000 GMT 28 January 1986, a low pressure area formed offshore of New Jersey with northwesterly flow in eastern U.S. and the system gradually moved northward along the Atlantic coast. During its northward progress, the low quickly deepened but the direction of the flow in the southeastern U.S. remained essentially the same. The generation and deepening of the low are part of the Type-B cyclogeneses offshore of the east coast as categorized by Miller (1946) and discussed by Dirks *et al.* (1988).

Flights of the NCAR Electra for mission R6 were performed at about 1300 GMT 28 January. Four research stations A-D (labeled in Figure 2 of Wayland and Raman, 1989) were flown approximately crosswind to obtain the detailed structure of the MBL over this region. In addition, SST along this flight track was measured to determine its distribution in the offshore direction. The measured SSTs are shown in Figure 1 in which the four stations are also labeled. The measurements (within ±0.5°C) along a nearly straight line downwind of the coastline enable the use of a 2-D model for simulating this cold air outbreak case.

The model domain (see Figure 1) covers 160 grids in the x-direction (defined along the measured SST line) with a uniform horizontal grid size of 5 km. A uniform ground temperature of 263°K is prescribed on grids 1–10 and the observed SST at Station A (inner shelf) on grid 22, B (shelf break) on grid 33, C (the Gulf Stream core) on 47, and D (the eastern Gulf Stream wall) on 67. Outside the observation regions (east of the Gulf Stream, grids 67–160), a constant temperature is assumed, to simplify boundary conditions. The big temperature drop (about 20°C) at the coastline (grid 11) is because of the extremely cold air inland with a temperature of −10°C. The SST between grids 12 and 21 is estimated using NOAA-7 AVHRR satellite image.

The model is oriented by −15° (to the south) in order that its x-axis will coincide with the SST gradient line (see Figure 2 of Wayland and Raman, 1989). The CLASS sounding at 1200 GMT on 28 January 1986 at Wilmington (grid 10) is used to specify the upstream condition. Figure 2 shows the observed wind (after the orientation), potential temperature and relative humidity (RH). The observed u-component (thin solid line) increases rapidly between 2–4.5 km, showing strong baroclinity. A low-level jet is found below 1 km, with a maximum speed of about 14 m s^{-1}. This jet is believed to have been caused by the temperature contrast between ocean and land. In the orthogonal direction, the v-component shows less regularity and no strong wind shear between 2 and 4.5 km in the observed profiles, indicating that the primary baroclinity is in the offshore direction. Associated with

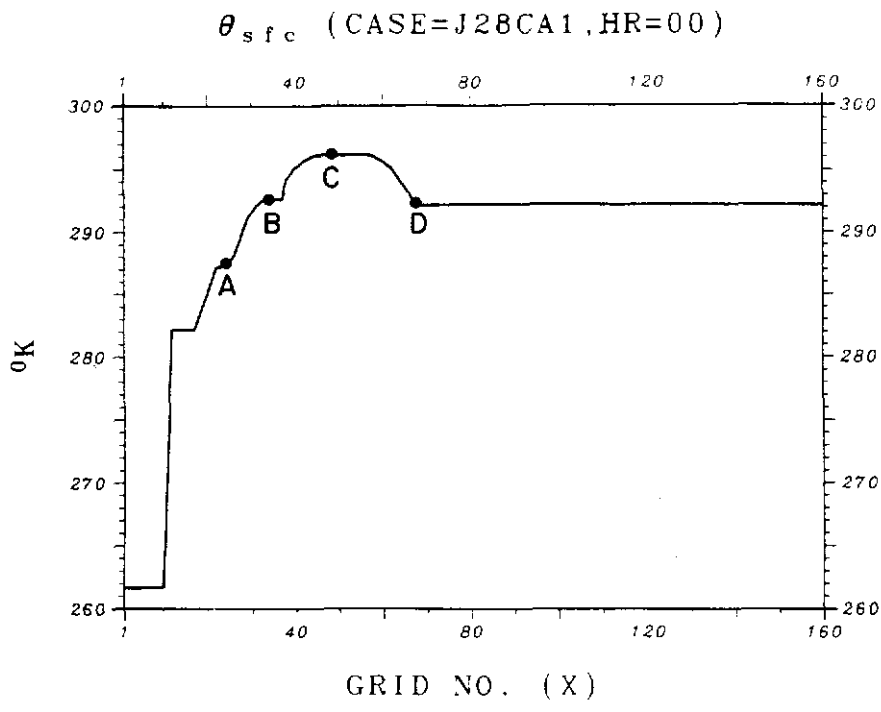

Fig. 1. Distribution of sea surface temperature along the flight track used as the initial condition in the 2-D model simulation. The model domain covers 160 grids in the x-direction (defined along the measured SST line) with a uniform grid size of 5 km. Ground temperature of 263°K is prescribed on grids 1–10 and the observed SSTs (Wayland and Raman, 1989) at Station **A** (inner shelf) on grid 22, **B** (shelf break) on grid 33, **C** (Gulf Stream core) on 47 and **D** (eastern Gulf Stream wall) on 67.

the baroclinic layer is a layer of stronger stratification. Below this layer, the air is well mixed within the lowest 700 m, indicating this to be the height of the PBL over land at 1200 GMT (0700 LST). Above the stable layer (4.5 km), there is a less stable layer of about 3.5 km thickness, above which the upper stratosphere is situated with a vertical gradient larger than 12°C km^{-1} in potential temperature. For this strong cold air outbreak, the atmosphere is very dry except near the surface as indicated by the RH profile in Figure 2.

It is clear that the non-uniform v-shear in Figure 2 would give very large temperature gradients if the thermal wind relation were used in the initialization. For example, the v-shear in the middle layer could imply a potential temperature drop of more than 20°C to the eastern boundary (~1000 km) if the thermal wind relation $\partial\theta/\partial x = (f\theta/g)\,\partial V_g/\partial z$ is retained. After the orientation, the u component above the baroclinic layer (2–4.5 km) is larger than 40 m s^{-1}, with a maximum wind speed of about 50 m s^{-1}. The pressure gradient inferred from the 500 mb pressure chart of the synoptic weather on this day, however, indicated a geostrophic wind of only 30–35 m s^{-1}. Therefore, the wind speed in the observed profiles was slightly reduced and the wind profile made more uniform so as to be

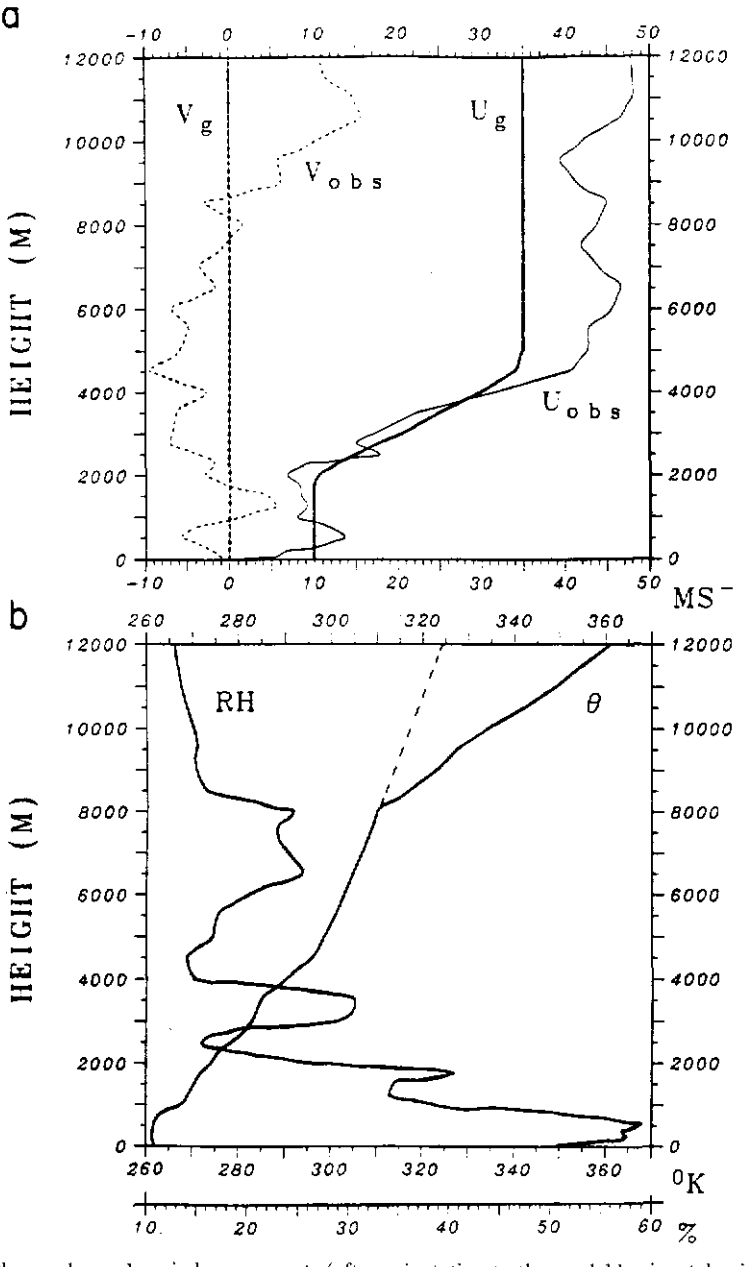

Fig. 2. Observed u and v wind components (after orientation to the model horizontal axis), potential temperature (θ) and relative humidity (RH) at Wilmington, North Carolina at 1200 GMT 28 January 1986 during an offshore cold air outbreak. The observed wind profiles are somewhat simplified to be geostrophic and are used as initial conditions (bold lines) in the 2-D model simulation.

TABLE I

Numerical experiments for 2-D simulations of the January 28 cold air outbreak during GALE IOP-2 (1986). The modified Blackadar formulation (denoted as BL) is used to determine eddy mixing length

Case	PBL closures	Geostrophic wind	Tropopause
J28CA1	E-ϵ with BL (level 2.5)	Baroclinic	Yes
J28CA2	E-ϵ with BL ($P_{rt} = 1$)	Baroclinic	Yes
J28CA3	E-ϵ with BL (level 2.5)	Baroclinic	No
J28CA4	E-ϵ with BL (level 2.5)	Barotropic	Yes

geostrophic. The v-component was set to zero close to its observed average value, and the strong u-shear between 2 and 4.5 km was retained. The strong middle-level shear of the geostrophic wind component U_g (in the direction normal to the coastline) is characteristic of the synoptic conditions. The wind field is then adjusted by the 1-D PBL model using the Ekman-gradient wind equations (Huang and Raman, 1988). The observed temperature and moisture profiles are frozen during the adjustment procedure for the wind. The thermal wind relation is then assumed to specify $\partial\theta/\partial y$, but there is no gradient in the y-direction (nearly parallel to the coastline) for other variables.

Table I gives a description of the model runs. For all the simulations, there are 33 vertically stretched grids, about half of which are used within the PBL for better resolution. All the simulations (J28CA1–4) are integrated from 0 to 24 model hour (starting from 1200 GMT January 28). The diurnal effect over the ground is not considered since it is not a focus of this study; rather, a neutral surface layer is assumed. Radiation and subgrid cloud effects are also neglected. Case J28CA1 is a control experiment in which the observations (Figure 2a,b) are used to initialize the model. In all the 2-D case simulations, the E-ϵ model with the modified Blackadar formulation for eddy mixing length (denoted as BL) is used to account for PBL turbulent transfer. Case J28CA2 is similar to J28CA1 except that the inverse Prandtl number (defined as $P_{rt} = K_\theta/K_M$) is assumed to have a constant value of unity as used in the E-model. The other two cases J28CA3–4 are for sensitivity tests. In the case of J28CA3, the tropopause and a part of the stratosphere were replaced with a layer of weaker stabilization (dashed line in Figure 2b). This case is used to investigate the effect of the tropopause on the dynamics of the flow at the upper levels and in the PBL. The last case J28CA4 for offshore flow assumes a barotropic atmosphere with a constant geostrophic wind ($U_g = 10\,\mathrm{m\,s^{-1}}$ and $V_g = 0\,\mathrm{m\,s^{-1}}$) but still uses the observed profiles of temperature and moisture. The results from the barotropic flow will reveal the effect of the baroclinity in J28CA1.

3. The Numerical Results

A. Mesoscale circulations

Time evolutions of the maximum and minimum vertical velocities (i.e., W_{max} and W_{min}) over the ocean for cases J28CA1–4 are plotted in Figure 3 to compare the

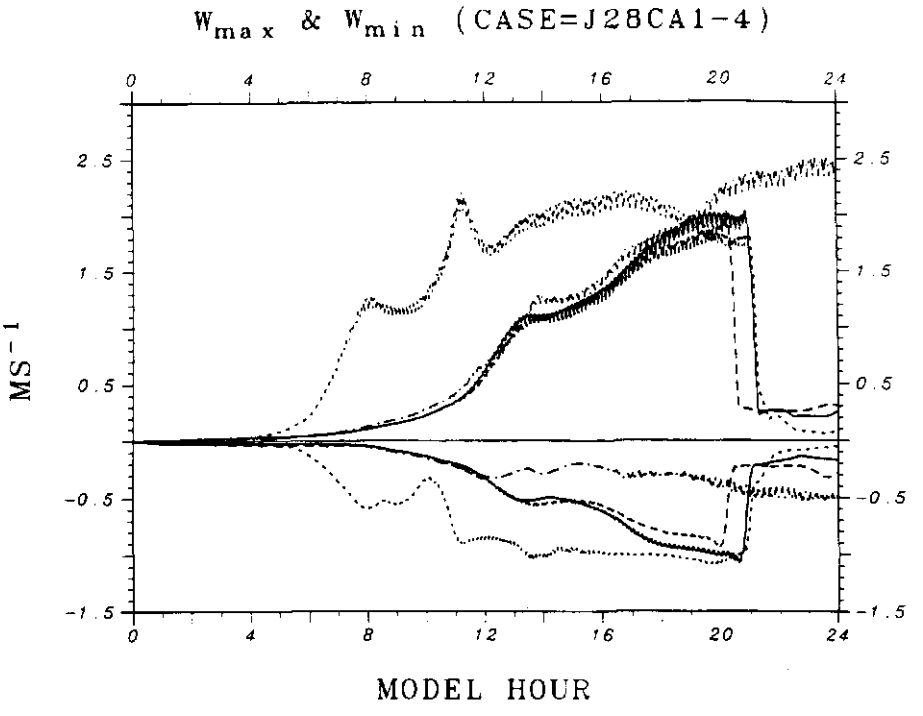

Fig. 3. Time evolutions of oceanic domain maximum and minimum vertical velocities for offshore cases J28CA1 (solid lines), J28CA2 (shorter dashed), J28CA3 (longer dashed) and J28CA4 (dotted-dashed).

different phases of the circulations. It can be seen that the circulation system for the case J28CA2 (with a constant Prandtl number of unity) develops earliest (before 8 h) among the four cases. At about 21 h, the three cases J28CA1–3 (for baroclinic flow) exhibit a sharp decrease in the updraft intensity (i.e., the W_{max}), but the updraft for J28CA4 (barotropic case) is still developing. This sharp decrease is because of the movement of the circulation front out of the model domain at this time. Movement of this front is faster in the baroclinic flow than in the barotropic case. The intensities of the associated updrafts in the circulation front, however, are similar, indicating that the updrafts could be mainly in response to the low-level convergence. On the other hand, reducing the strong stratification of the stratosphere (case J28CA3) appears to have minor effects on the development of the circulation system.

Figure 4 shows the circulation system at 6 h for the case J28CA1. At 6 h, the MBL over the Gulf Stream core has developed to about 2300 m, in good agreement with the observations (see Table II of Wayland and Raman, 1989). The MBL height increases offshore east of the coastline and becomes uniform (about 1800 m height) east of the eastern edge of the Gulf Stream (grid 67). The increased offshore development of the MBL is also indicated by the observations. A low-level jet (regarded as part of the circulation front) is found ahead of the Gulf

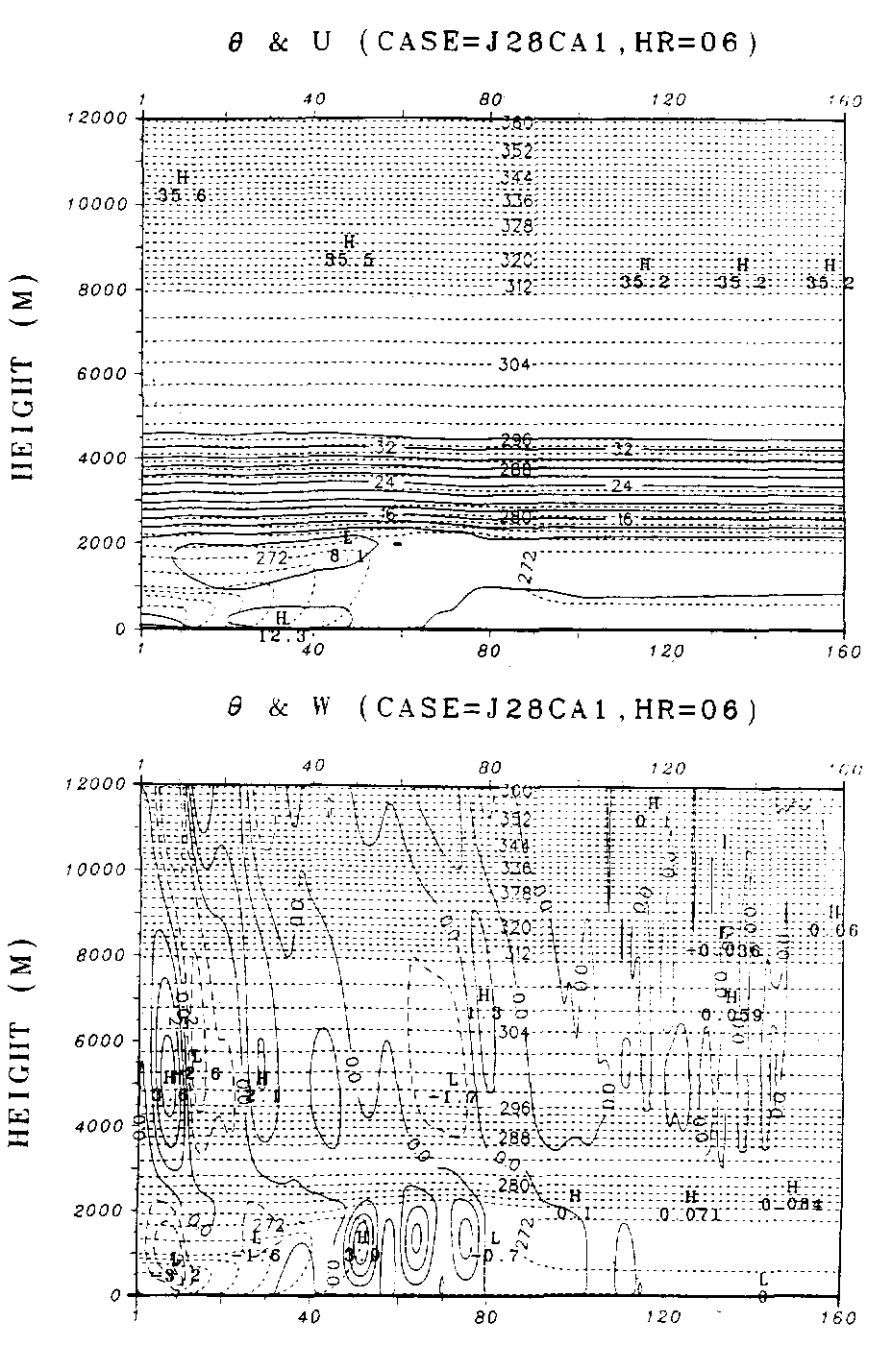

Fig. 4. The results for θ (shorter dashed lines), u (solid) and w (longer dashed and solid) at 6 h for case J28CA1 (offshore baroclinic flow). The horizontal axis in each panel is defined as the grid number (with a uniform grid interval of 5 km). Contour intervals are 2°K for θ, 2 m s^{-1} for u and 1 cm s^{-1} for w.

Stream core (grid 47) with a maximum wind speed of 12.3 m s^{-1}. Downward motions (on the order of several centimeters per second) exist west of the front, while slightly stronger upward motions appear to the east of the front. The location of the major updraft (at about grid 50) indicates the degree of upward penetration of the front. Locations and the heights of the jet and the upper-level return perturbation flow are close to the observations (see Figure 7 of Wayland and Raman, 1989).

The circulation system becomes much stronger at 12 h (Figure 5). Baroclinic waves that begin to appear downwind of the Gulf Stream are exhibited by the reversed phases of the upper and lower level ridges and troughs of vertical motions. The baroclinic waves tilt upstream, indicating the upward radiation of wave energies. The waves are also propagating downstream as evident in the multi-cells of a vorticity street. At this time, another low-level jet forms just west of the strongest low-level updraft (around grid 95), and the jet at the inner shelf moves farther offshore to the Gulf Stream core.

As the circulation front moves farther offshore, the u-shear layer is more disturbed due to the increasing boundary-layer destabilization, which in turn triggers the cloud development because of more convective instability. This is evident in the flow at 15 and 18 h as shown in Figures 6 and 7. It can be seen that at 18 h, the low-level updraft already penetrates out of the bottom of the u-shear layer. This penetration leads to the lifted isentropics which induce the upper-level waves. The baroclinic waves (at 12 h) behave like mountain waves since they are triggered by a density mountain. At 21 h (not shown), the circulation front has reached the eastern model boundary but the maximum MBL height is still less than 2.5 km. The vertical motions at low levels and at the levels just above the u-shear layer begin to be in phase by 18 h and develop to a height of about 8 km. The upper-level baroclinic waves propagate offshore with time in accordance with the mobile density mountain.

Figures 4–7 clearly exhibit a continuous development of the MBL updrafts and the movement of the circulation front for an offshore undisturbed ambient condition. The moving speed of the front (estimated from these figures) is about 9.26 m s^{-1}, which is slightly smaller than the near-surface geostrophic wind speed of 10 m s^{-1}. It should be noted that even after the 21 h integration, the maximum height of the MBL over the Gulf Stream region is still below 2.5 km. However, the PBL over land is shallow (about 500–700 m height). Low-level turbulence over land is obviously suppressed by the stable stratification of the sheared layer in combination with the cold air advection upstream.

Our previous modelling study using cloud parameterization only for liquid water has also shown the formation of a cloud band in response to the frontal updrafts (Huang and Raman, 1990a). The current model separates the liquid water into cloud water and rain water. Thus, it is expected that the configuration of clouds will be more reasonable. At 6 h, clouds (not shown) develop in the region extending from the Gulf Stream core to about grid 80, but no rain occurs. The

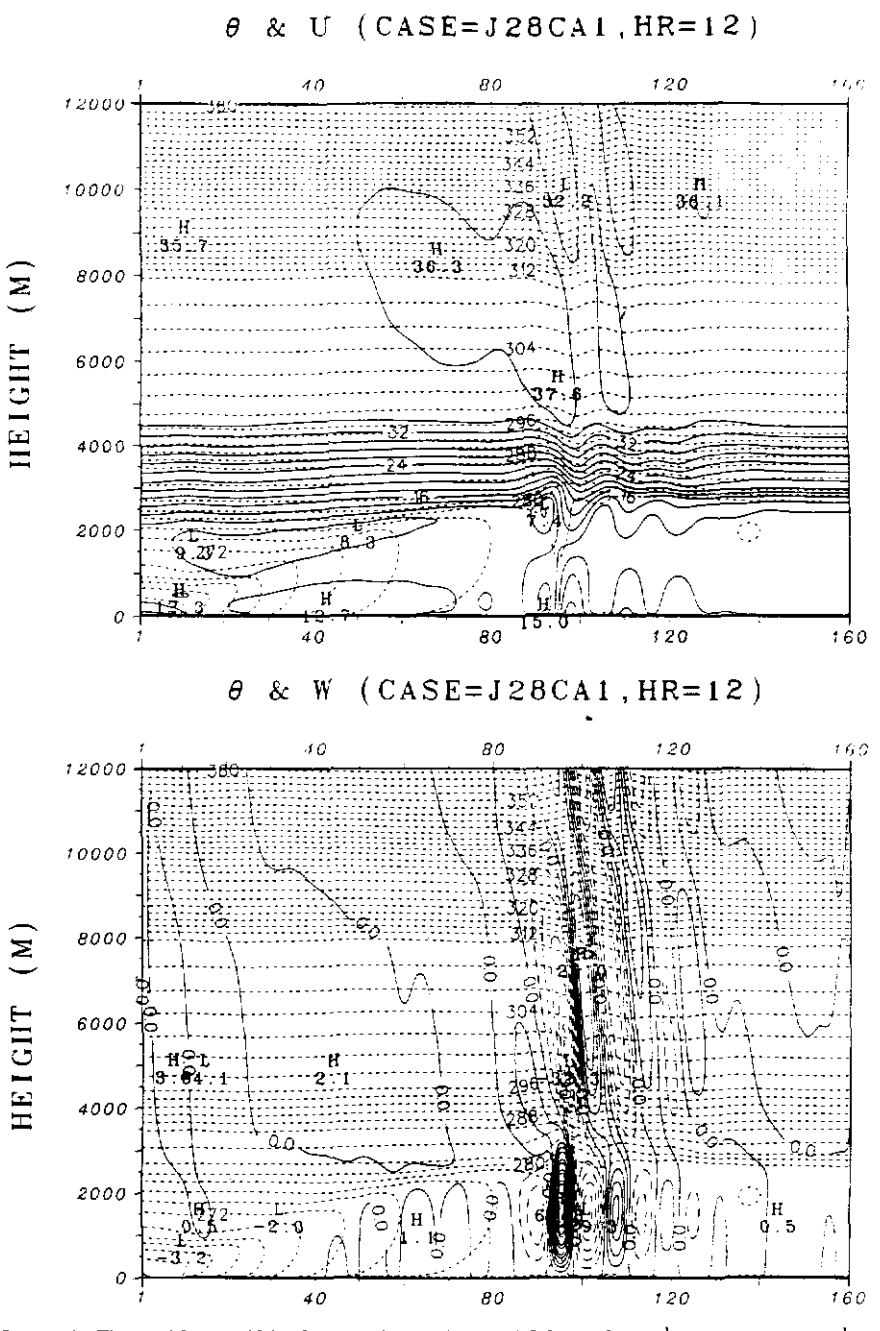

Fig. 5. As in Figure 4 but at 12 h. Contour intervals are 2°K for θ, 2 m s^{-1} for u and 5 cm s^{-1} for w.

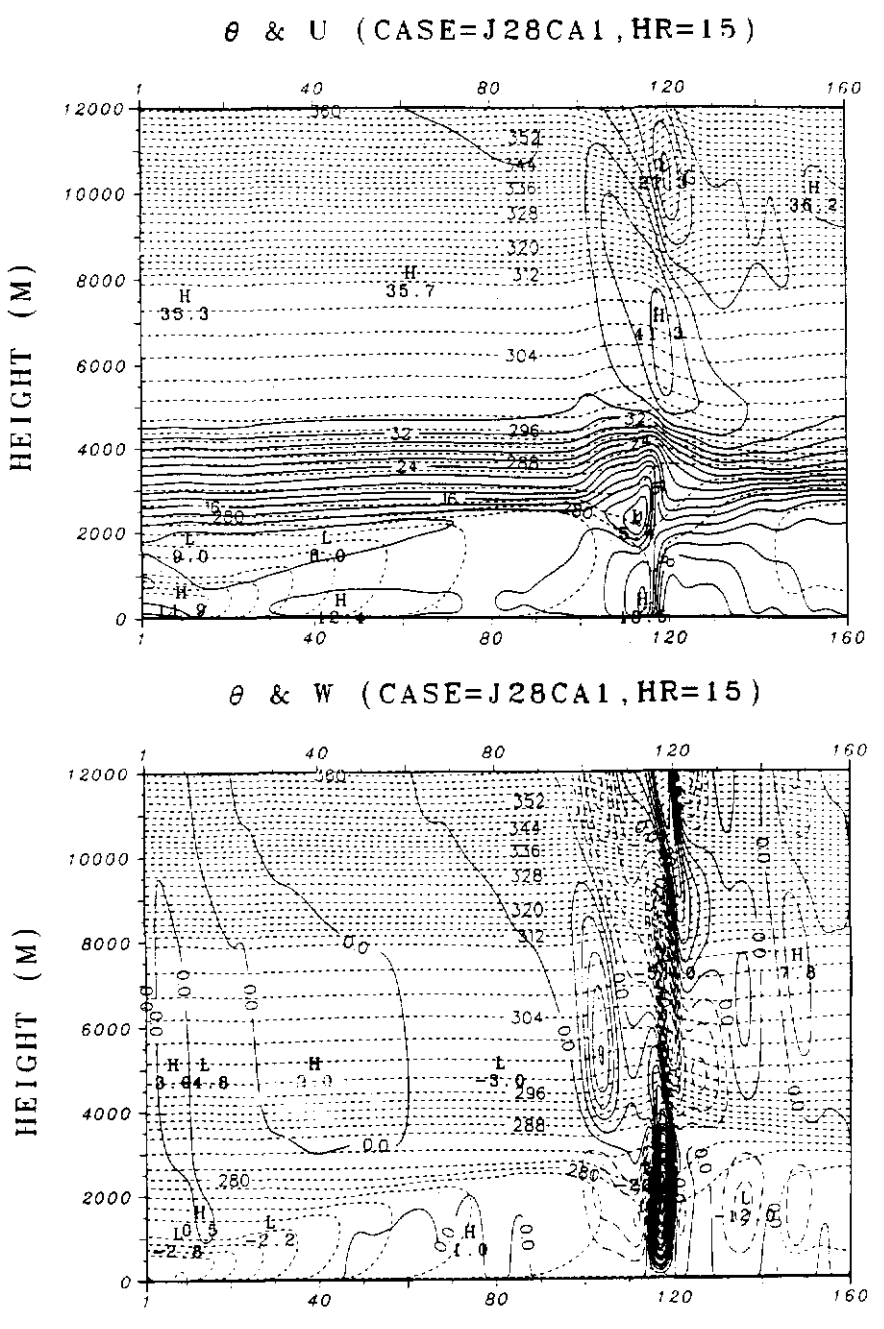

Fig. 6. As in Figure 4 but at 15 h. Contour intervals are 2°K for θ, 2 m s^{-1} for u and 5 cm s^{-1} for w.

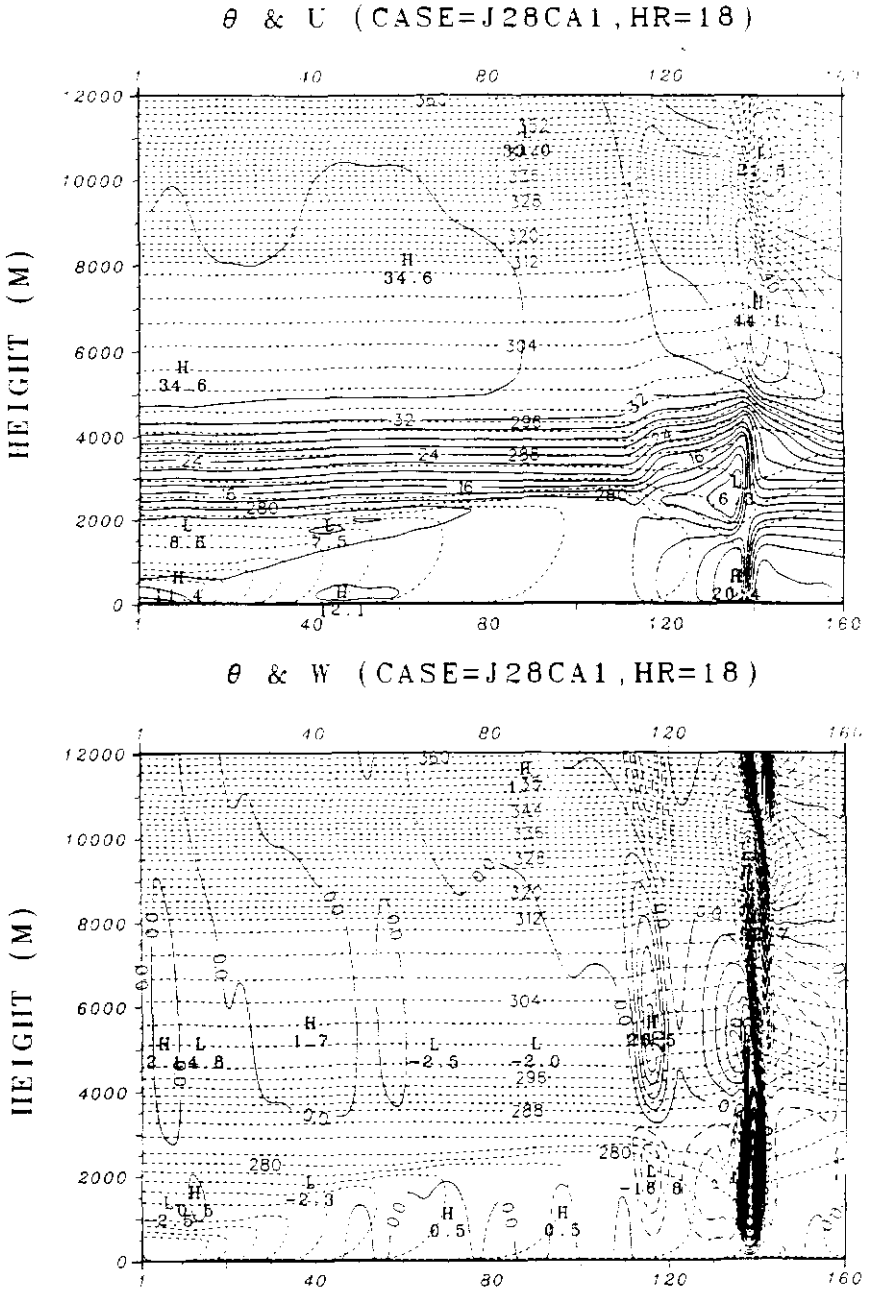

Fig. 7. As in Figure 4 but at 18 h. Contour intervals are 2°K for θ, 2 m s^{-1} for u and 5 cm s^{-1} for w.

clouds are very light (less than 0.1 g kg^{-1}) and shallow (within a height of 2.5 km) with a base height below 200 m. These features were observed during the experiment (Wayland and Raman, 1989).

As the circulation front passes the eastern edge of the Gulf Stream, the clouds begin to develop quickly downwind. At 12 h, rain associated with these clouds occurs (not shown). Both the cloud and rain waters are within 4 km height. With the circulation front located farther offshore, the clouds become denser and develop to a height of 5 km (Figure 8). A single prominent rainband appears around grid 117 at 15 h and around grid 140 at 18 h, at an average height of about 4 km. At 21 h (not shown), the cores of the cloud and rain bands reach the model boundary in response to the movement of the circulation front. The modeled dense cloud and rain bands appear east of the Gulf Stream. This is in general agreement with the distribution of clouds from the satellite imagery (Wayland and Raman, 1989).

B. Turbulence in the MBL: Influence of the Prandtl number

Turbulence structure in the MBL during a cold air outbreak over the ocean is examined in this section. In addition, the influence of the Prandtl number on the model prediction will be discussed. The sensitivity test, case J28CA2, assumes a constant Prandtl number of unity in the turbulence closure, otherwise this case is identical to J28CA1.

For comparisons, the circulation systems at 15 and 21 h for case J28CA2 (with $P_{rt} = 1$) are shown in Figure 9. It can be seen that the u-perturbation for this case is stronger than that for J28CA1 (with the level 2.5 formulation). This feature is found in the evolution of the updrafts as well (Figure 3) although the speeds of the cloud and rain bands for these two cases are approximately the same (not shown). At the same time, the MBL for case J28CA2 is not as convective as the one for J28CA1 (see Figure 7). This is evident in the increased downstream tilting of the isentropic contours in Figure 9, indicating the larger effect of cold air advection in the MBL for J28CA2. In this case, relatively stronger advection offsets the effects of turbulent transfer, which is mainly due to smaller eddy diffusivities for heat for J28CA2 as compared to J28CA1 (with the level 2.5 formulation). With larger tilting of the thermal structure of the MBL for J28CA2, the development of clouds (not shown), however, is stronger.

Figure 10 shows the distributions of surface-layer turbulence parameters u_*, θ_*, w_*, and q_* at 6 h for cases J28CA1 (bold lines) and J28CA2 (dashed lines). Since the same surface-layer similarity has been applied to the two cases, the surface-layer turbulence parameters have nearly the same distributions. East of the Gulf Stream, these parameters vary little in space. Larger magnitudes of these parameters occur near the Gulf Stream core, producing the higher MBL. The friction velocities u_* over the Gulf Stream core and east of the Gulf Stream are about 0.5 and 0.38 m s^{-1}, respectively. These values compare well with the observations of 0.55 m s^{-1} at grid C (Gulf Stream core) and 0.40 m s^{-1} at grid D

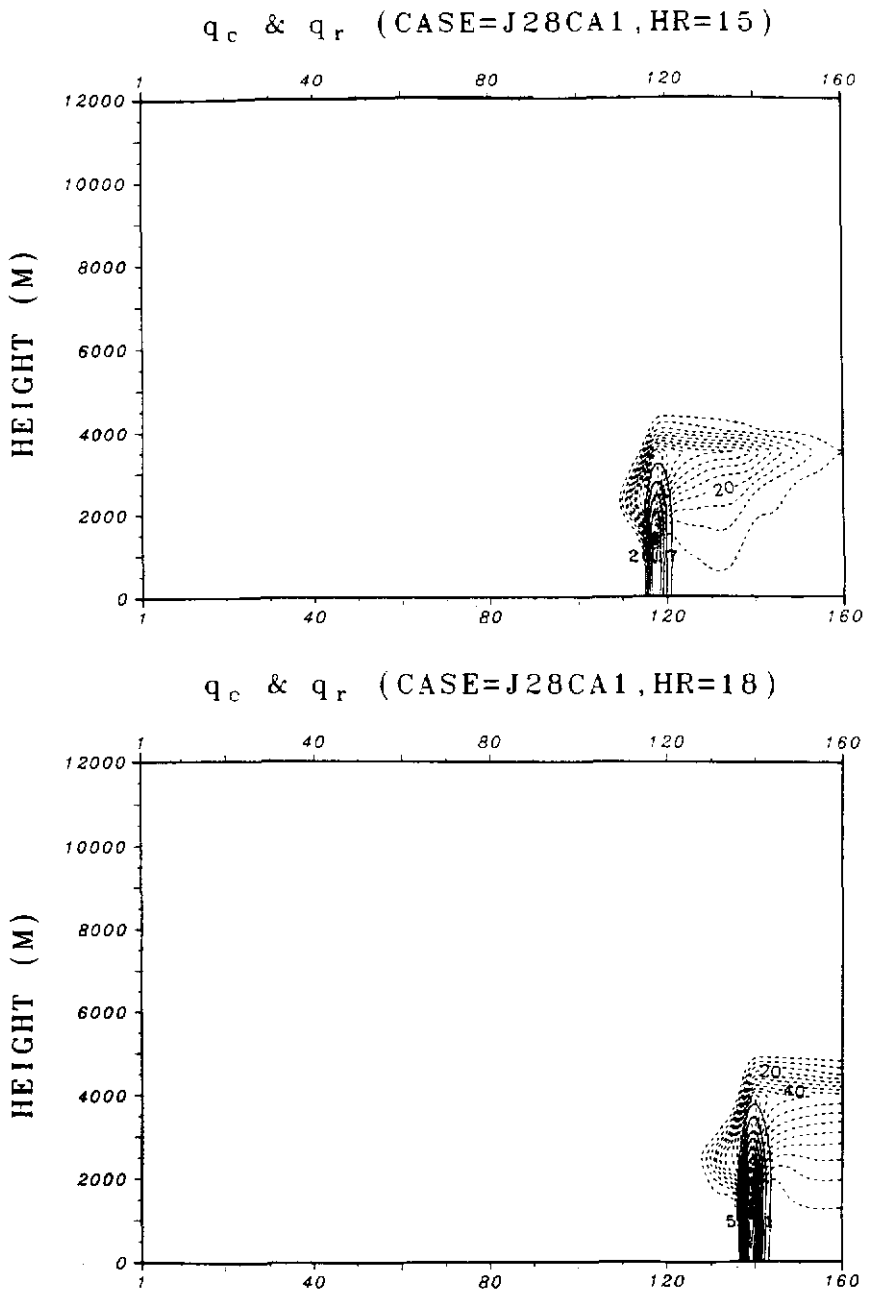

Fig. 8. The results for q_c (dashed lines) and q_r (solid) at 15 and 18 h for case J28CA1 (offshore baroclinic flow). Contour intervals are 0.05 g kg^{-1} for both q_c and q_r.

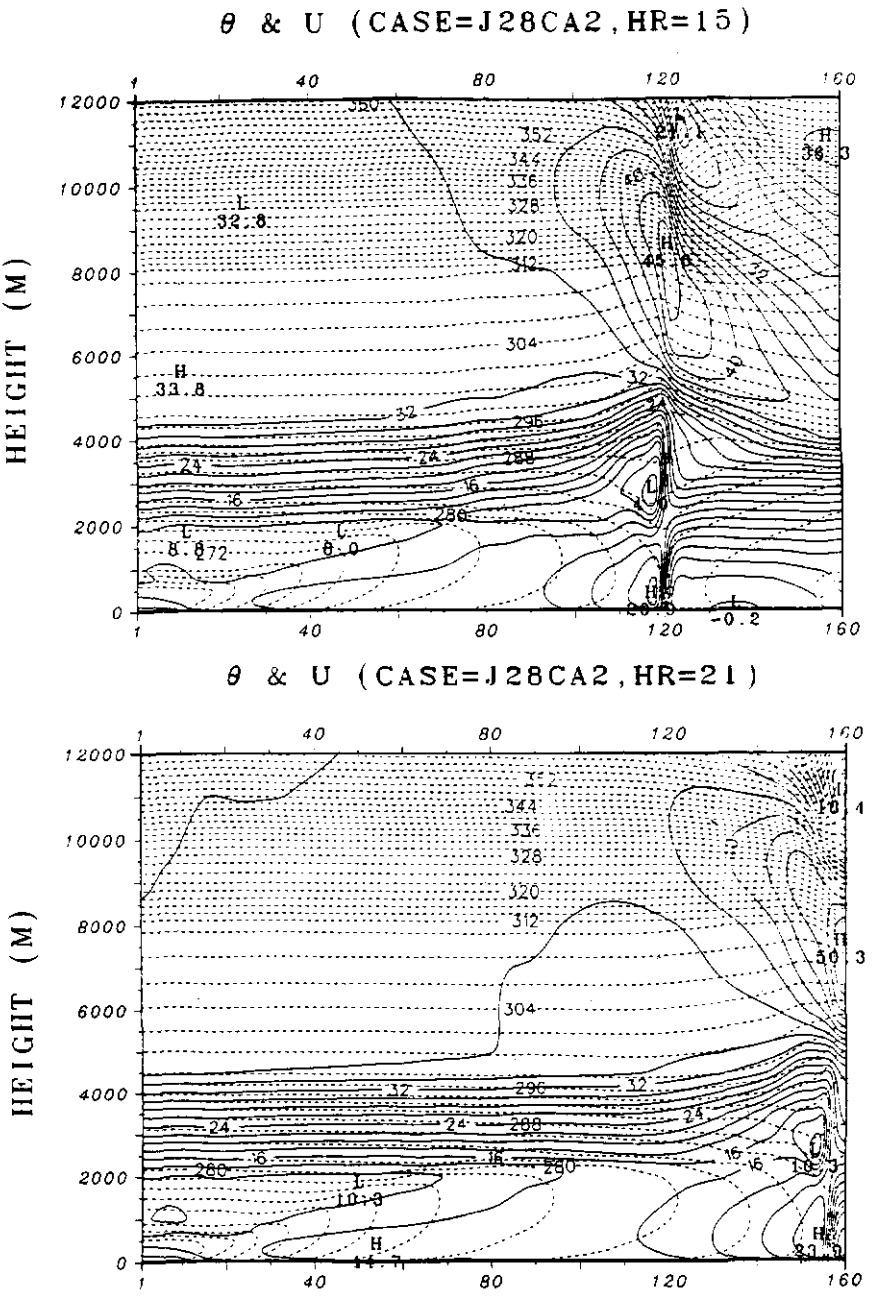

Fig. 9. The results for θ (shorter dashed lines) and u at 15 and 21 h for case J28CA2 (offshore baroclinic flow with a constant eddy Prandtl number). Contour intervals are 2°K for θ and 2 m s^{-1} for u.

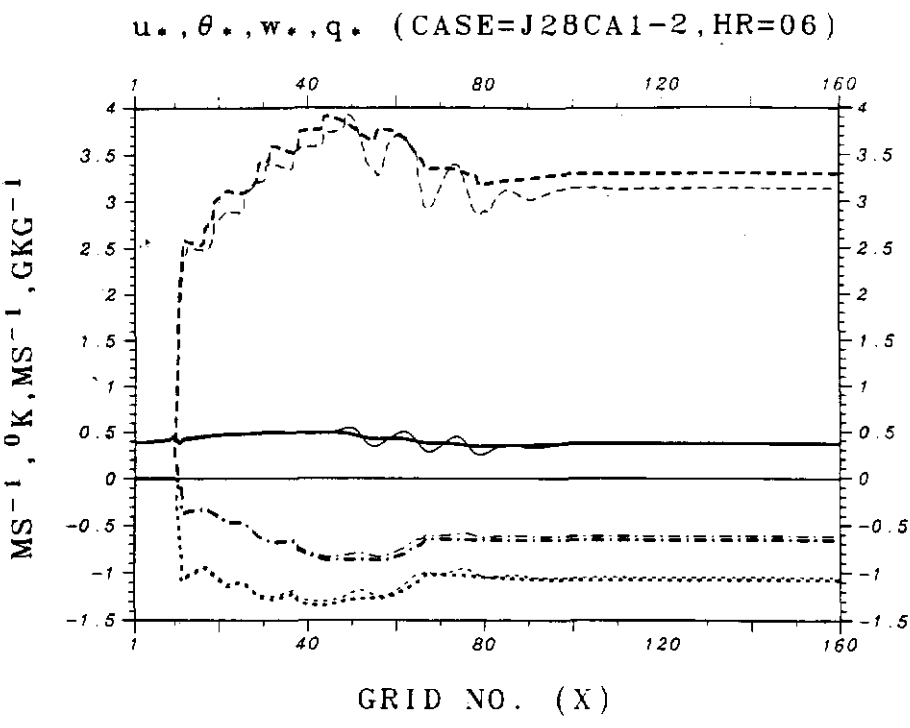

Fig. 10. Distributions of surface-layer turbulent flux parameters at 6 h for cases J28CA1 (bold lines) and J28CA2 (thin). Turbulent parameters are surface-layer friction velocity u_* (solid lines), flux potential temperature θ_* (shorter dashed), convective velocity w_* (longer dashed) and flux moisture q_* (dotted-dashed), in units of m s^{-1}, °K, m s^{-1} and g kg^{-1}, respectively.

(east of the Gulf Stream) (see Table II of Wayland and Raman, 1989). It can be seen that the variations of these parameters approximately resemble the distribution of the SSTs. Values of u_*, θ_* and q_* for the two cases are quite similar. This indicates that the surface layer is not significantly influenced by the difference in the Prandtl numbers above this layer. Thus, stronger cloud development for J28CA2 appears to be due to different turbulent transfers at upper levels of the MBL.

Before further comparisons, it would be appropriate to discuss turbulent heat transfers in the MBL for J28CA1 and compare them with the observations. Figure 11 shows the vertical distributions of sensible and latent heat fluxes at 6 h. It can be seen from this figure that the thickness of the modeled entrainment layer is about 20–30% of the MBL depth. The maximum value of the negative sensible heat flux is about 20% of the surface-layer value, similar to the 1-D model results discussed in Part I. Within the MBL, the sensible heat flux decays almost linearly with height, but the latent heat flux is approximately constant except for a rapid decrease in the entrainment layer. These are common features observed in a well-mixed convective boundary layer. Location of the maximum total surface-layer heat flux (about 1750 W m^{-2}) is found at the Gulf Stream core (grid 47). The

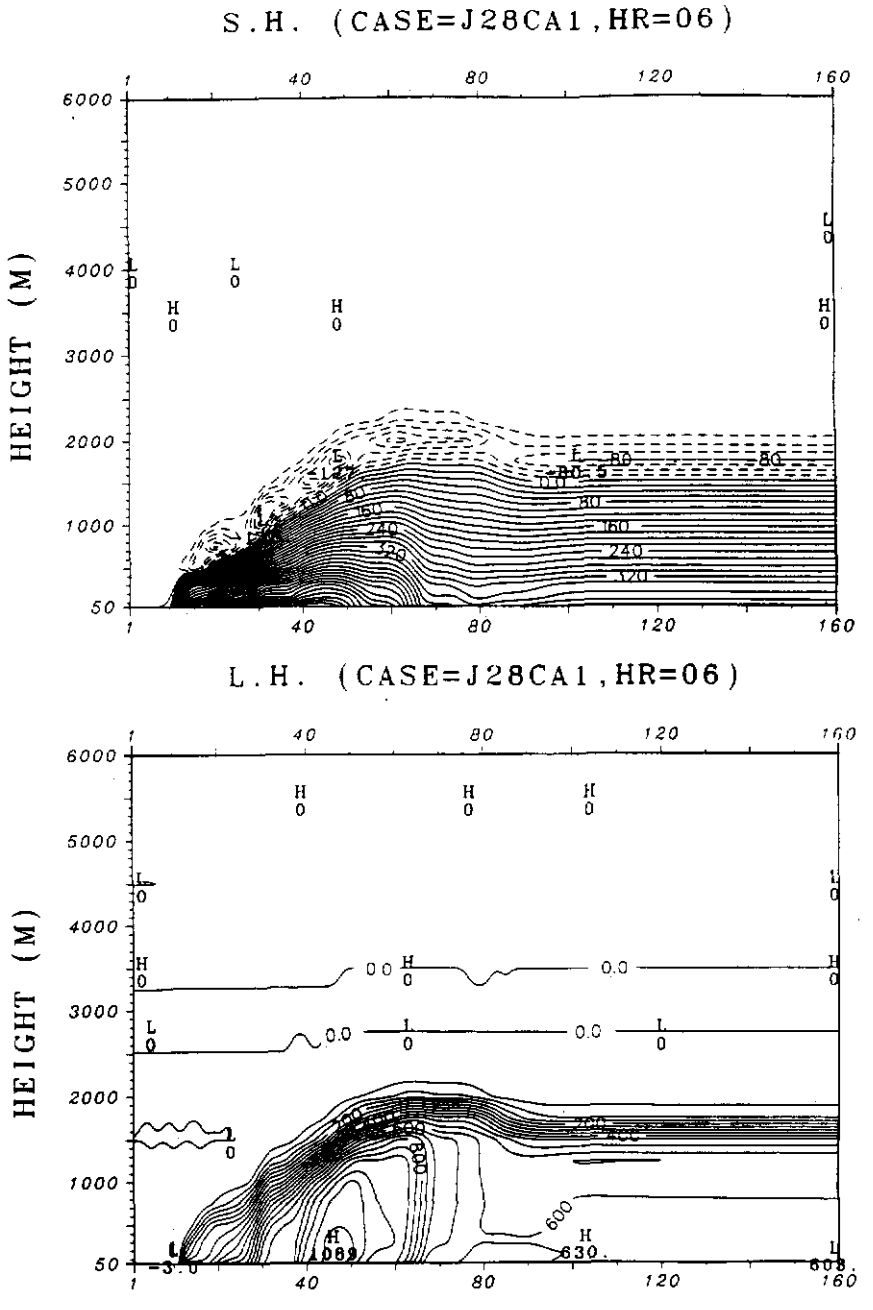

Fig. 11. Turbulent sensible and latent heat fluxes at 6 h for case J28CA1. Contour intervals are 20 W m^{-2} for sensible heat flux and 50 W m^{-2} for latent heat flux.

modeled value of the maximum surface-layer heat flux is consistent with observations. A value of 1200 $W m^{-2}$ was observed west of the Gulf Stream front (Wayland and Raman, 1989). The distributions of the modeled heat flux agree well with observations, showing decreasing trends west of the inner shelf (grid 22) and east of the Gulf Stream (grid 67). Since initial air temperatures in the model are horizontally homogeneous, the model air-sea temperature difference could be larger than actually exists and could result in heat fluxes larger than the observations at 6 h. Another possible reason could be that upstream conditions of mean flow are assumed to be constant during integration, but the CLASS soundings at Wilmington at 1800 GMT (6 model hour) show a weakening of the cold air intensity due to diurnal effects (about 7–8°C warming). This also leads to a slight decrease in the observed low-level wind speed.

Figure 12 shows the TKE distributions at 6 h for the two cases (J28CA1 and J28CA2). It can be seen that the general structures of the TKEs for the two cases are similar, but a constant P_{rt} of unity appears to yield more disturbed upper-level waves as compared to the level 2.5 one. The TKE distributions in the surface layer are consistent with the observations, giving a maximum value of 5 $m^2 s^{-2}$ near the Gulf Stream core (grid 47) (Wayland and Raman, 1989). Over the constant SST region east of the Gulf Stream (grid 67), TKEs for the two cases differ much less. The maximum MBL height inferred from the TKE for J28CA1 is slightly larger (about 200 m) than that for J28CA2, which could be attributed to the larger eddy diffusivities (not shown). The typical magnitudes of eddy diffusivity for heat (i.e., K_θ) for J28CA1 (with the level 2.5 formulation) is about 1.9 times that for J28CA2 (assuming $K_M = K_\theta$), indicating the importance of the effects of thermal stability and wind shear in the determination of the Prandtl number. Despite the difference in their magnitudes, the distributions of K_θ for both cases are quite similar to those of their TKEs.

Comparisons between the profiles of TKE budgets for the two cases are also made. The TKE budgets over the land and over the oceanic region of maximum cloud water loading (denoted as TKE BD1 and TKE BD2, respectively) will be of particular interest. For TKE BD1, the two case results show similar vertical profiles with a balance between the turbulent dissipation and shear production (not shown). This is because of the assumption of a neutral surface layer over the land. Figure 13 shows the vertical profiles for TKE BD2 at 6 and 12 h for the two cases (J28CA1 and J28CA2). As in a typical CBL, at 6 h, positive buoyancy decreases linearly with height below the nondimensional MBL height of 0.8, above which entrainment associated with negative buoyancy and positive turbulent transport takes place (Figure 13a). Thus, the 2-D model prediction of the turbulence in the MBL before the cloud development is similar to the 1-D model results. With larger eddy diffusivities, larger magnitudes of the TKE budget components are found at various heights for J28CA1 (bold lines) as compared to J28CA2 (dashed lines). Maximum heights of the MBL deduced from the TKE budget components are approximately the same at 6 h for the two cases.

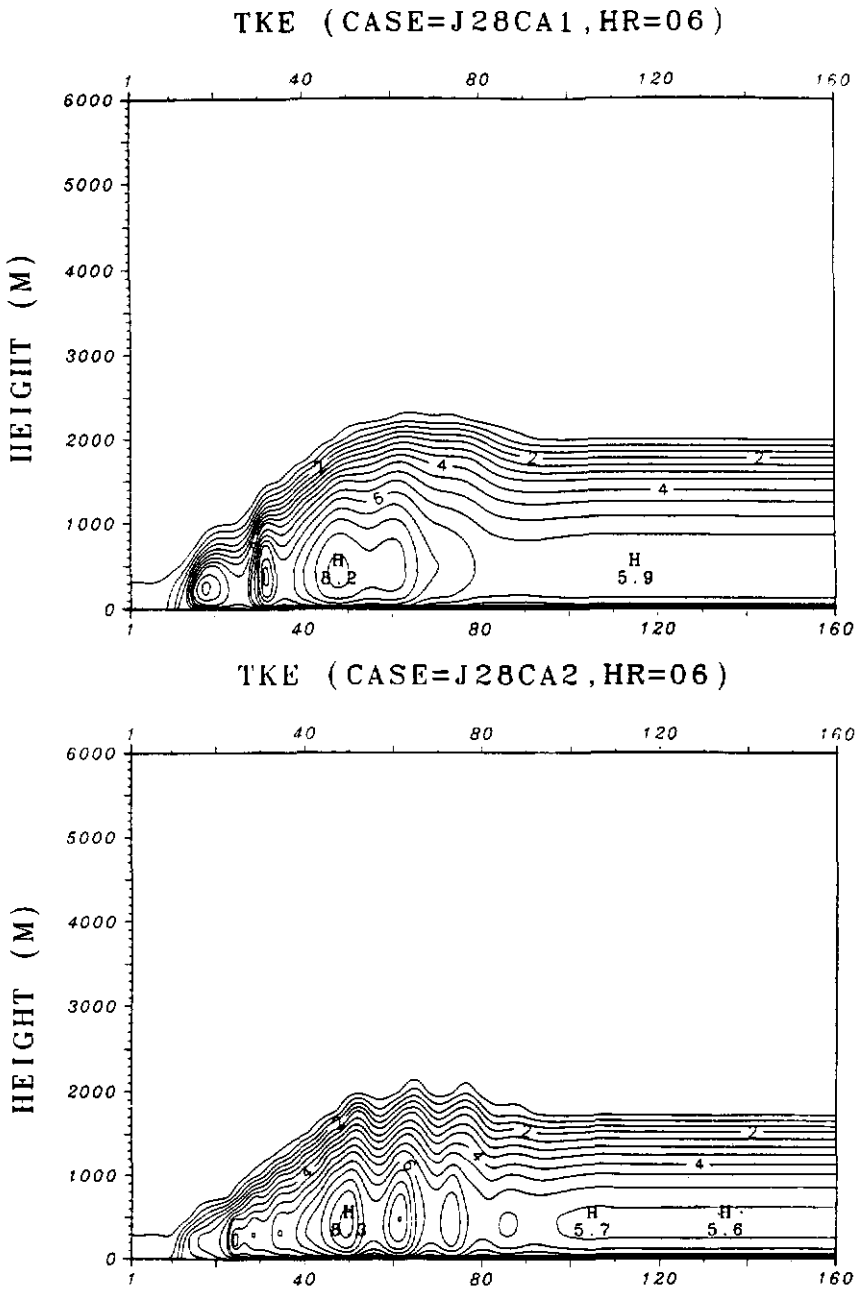

Fig. 12. TKE at 6 h for cases J28CA1 and J28CA2. Contour intervals are 0.5 m^2 s^{-2} for both cases.

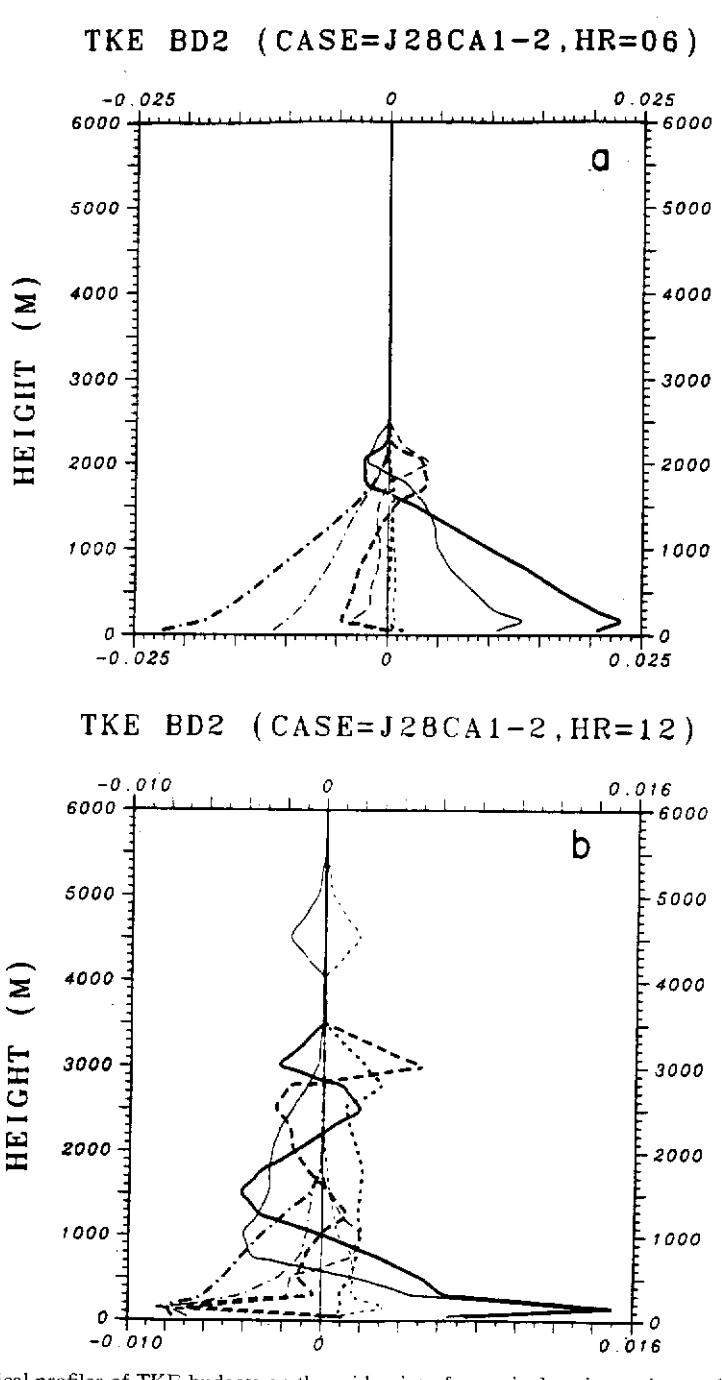

Fig. 13. Vertical profiles of TKE budgets on the grid point of oceanic domain maximum cloud water loading at (a) 6 h and (b) 12 h for cases J28CA1 (bold lines) and J28CA2 (thin). TKE budget terms are buoyancy (solid lines), shear production (shorter dashed), turbulent transport (longer dashed) and dissipation (dotted-dashed).

Results for the TKE BD2 differ greatly at 12 h for the two cases (Figure 13b). Similarity between each of the TKE budget components for the two cases is found only near the surface layer. Turbulence develops to a higher altitude for J28CA2 (thin lines) than for J28CA1 (bold lines). Also, J28CA1 gives a positive buoyant layer between 2 and 3 km (see bold solid line), but only a near neutral layer (between 3.5 and 4 km) is found for J28CA2. The upper-level buoyancy for the two cases is due to the cloud effects. Shear production just below this layer is prominent for J28CA1, but is much smaller for J28CA2. Entrainment occurs near the cloud top where overshooting of the clouds would lead to adiabatic cooling. It can be clearly seen that the entrainment layer for J28CA2 is at a level about 1.5 km higher than that for J28CA1. Thus, larger eddy diffusivities for the turbulence at the upper levels (as the level 2.5 case will give) do not ensure that clouds will develop to higher levels. Except near the cloud top where stable stratification leads to a dominant buoyancy term, the primary terms of the TKE budget components inside the clouds are less certain. This also implies that at least a 2-D model that includes advection effects is necessary to simulate the turbulence inside clouds accurately.

Global differences in the turbulence for the two cases can also be assessed by the domain distributions of the heat flux, e.g., Figure 14 for their sensible heat fluxes at 12 h. As can be seen, the distributions and magnitudes of the turbulent heat transfers over the Gulf Stream region for the two cases are still similar, but their differences increase remarkably at and downwind of the region of maximum cloud water loading (around grid 100). A significant negative buoyant layer between 3 and 5.5 km in the cloudy region for J28CA2 is consistent with the TKE budgets shown before. Downwind of this location (grid 100), similarity between the two cases no longer exists at 12 h. Compared to J28CA1, J28CA2 produces a thicker entrainment layer, especially far downstream. The intensity of the entrainment is also stronger downwind of the Gulf Stream region. The influence of the Prandtl number on the circulation system becomes important as the clouds begin to interact vigorously with the MBL.

C. Effects of the tropopause

The effect of the tropopause is investigated in the case J28CA3 with a layer of weaker stratification (4°C km^{-1}) above 8 km. Figure 15 shows the modeled circulation at 18 h. As can be seen, the low-level circulation is almost the same as that for J28CA1. The upper-level density mountain wavelength increases in the case J28CA3, however. This can be explained in terms of the dynamics of mountain waves (Smith, 1979) in a two-layer stratified atmosphere characterized by the Scorer parameter (a wavenumber) defined as $l^2 = N^2/U^2 - U_{zz}/U$, where N is the Brunt–Väisälä frequency and U the upstream wind speed. Replacing the tropopause with a layer of reduced stratification increases the wavenumber which in turn changes the phase of the mountain waves. Thus, the upper-level trough as seen in Figure 7 will not appear totally within the model domain since the wave-

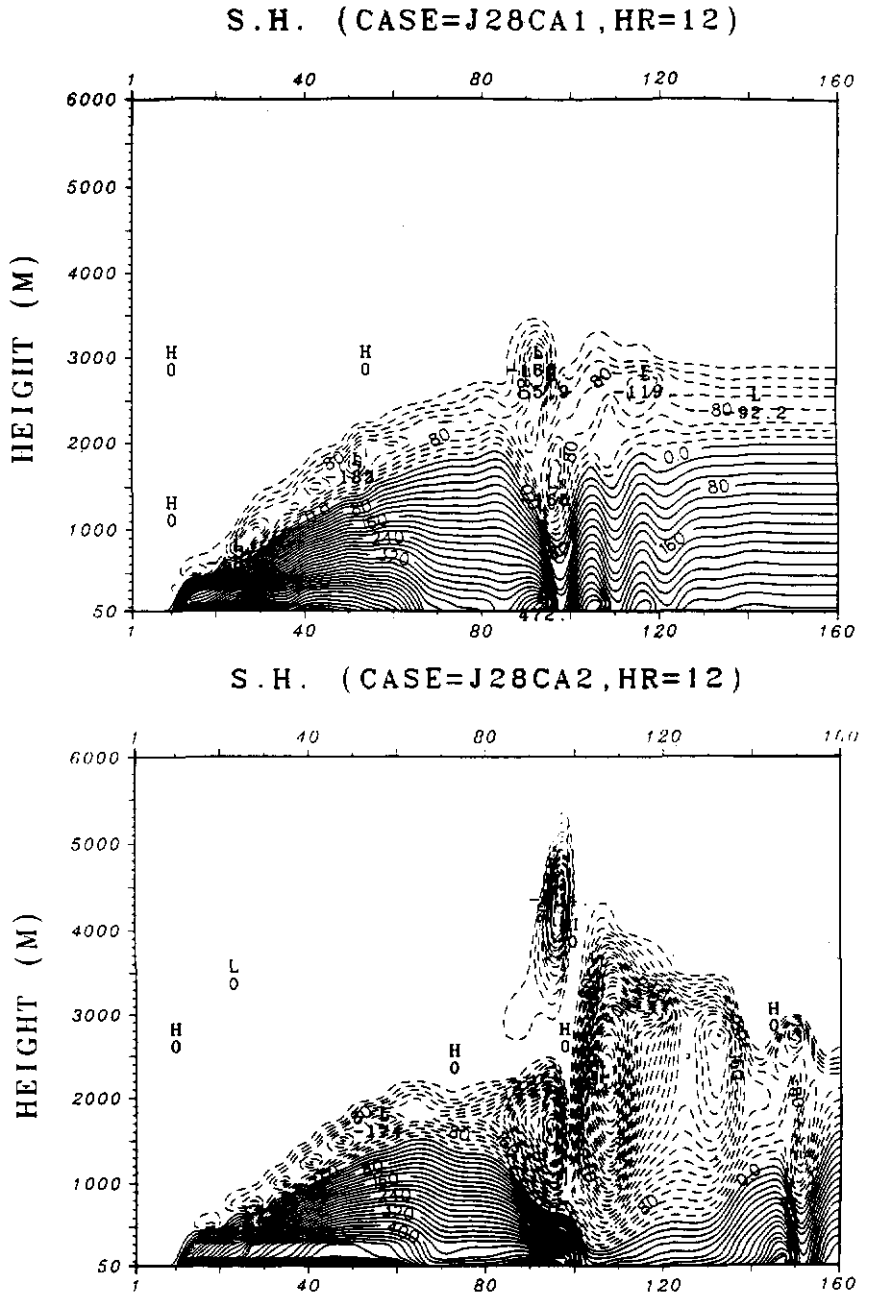

Fig. 14. The results for turbulent sensible heat flux at 12 h for cases J28CA1 and J28CA2. Contour intervals are 20 W m^{-2} for both cases.

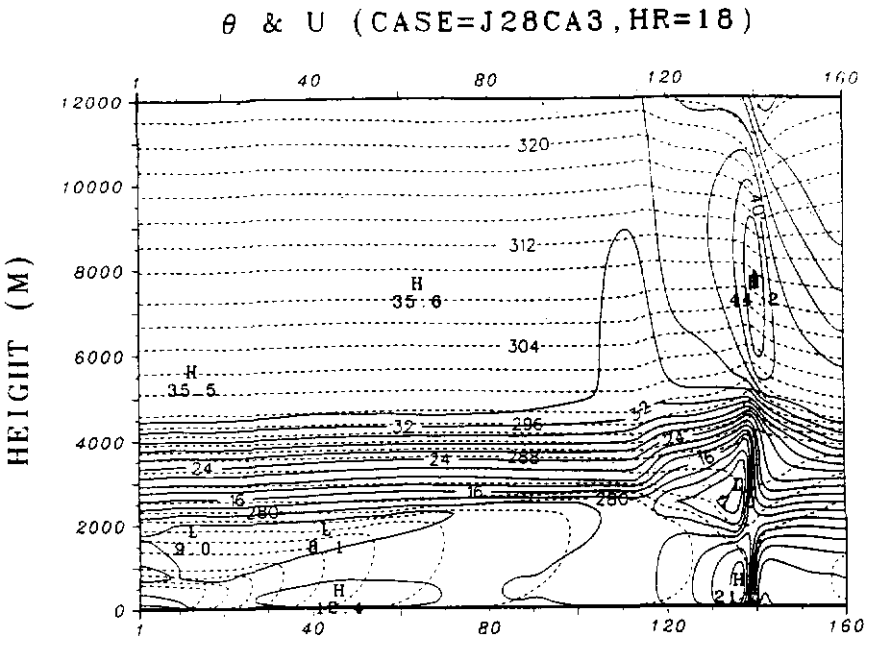

Fig. 15. The results for θ (shorter dashed lines) and u (solid) at 18 h for case J28CA3 (baroclinic flow without the tropopause). Contour intervals are 2°K for θ and 2 m s^{-1} for u.

length ($2\pi/l$) is about 11.2 km. In the evaluation of the Scorer number at 4.5 km, the term U_{zz}/U is dominant, being given by $(0-0.01)/(\Delta z_u U_g)$, where Δz_u is the half thickness of the u-shear layer. Thus, the results shown in Figures 7 and 15 agree with mountain wave theory. To verify the results, further, another experiment with a higher model top (16 km) was conducted. The results (not shown) produced the density mountain waves of full wavelength as mountain wave theory predicts.

D. Response to barotropic flow

Similar cases but with barotropic flow of constant stratification were investigated by Huang and Raman (1990a). It was found that the speed of the rainband downwind of the Gulf Stream was slightly slower than the speed of the mean flow. Figure 16 shows the results at 18 and 21 h for the case J28CA4. As estimated from this figure, the circulation front and the MBL updrafts move at a speed of about 7 m s^{-1}. This is smaller than the rainband speed of 9.26 m s^{-1} in baroclinic flow and is also smaller than the near-surface geostrophic wind of 10 m s^{-1}.

The circulation for barotropic flow is typical of breeze-type circulations, showing a low-level jet associated with upper-level perturbed return flow (Figure 16). Farther downwind of the Gulf Stream, the breeze intensifies more with stronger vertical motions (not shown). Heights of the cloud and rain bands also become larger as the front moves farther offshore (not shown). The cloud and rain bands

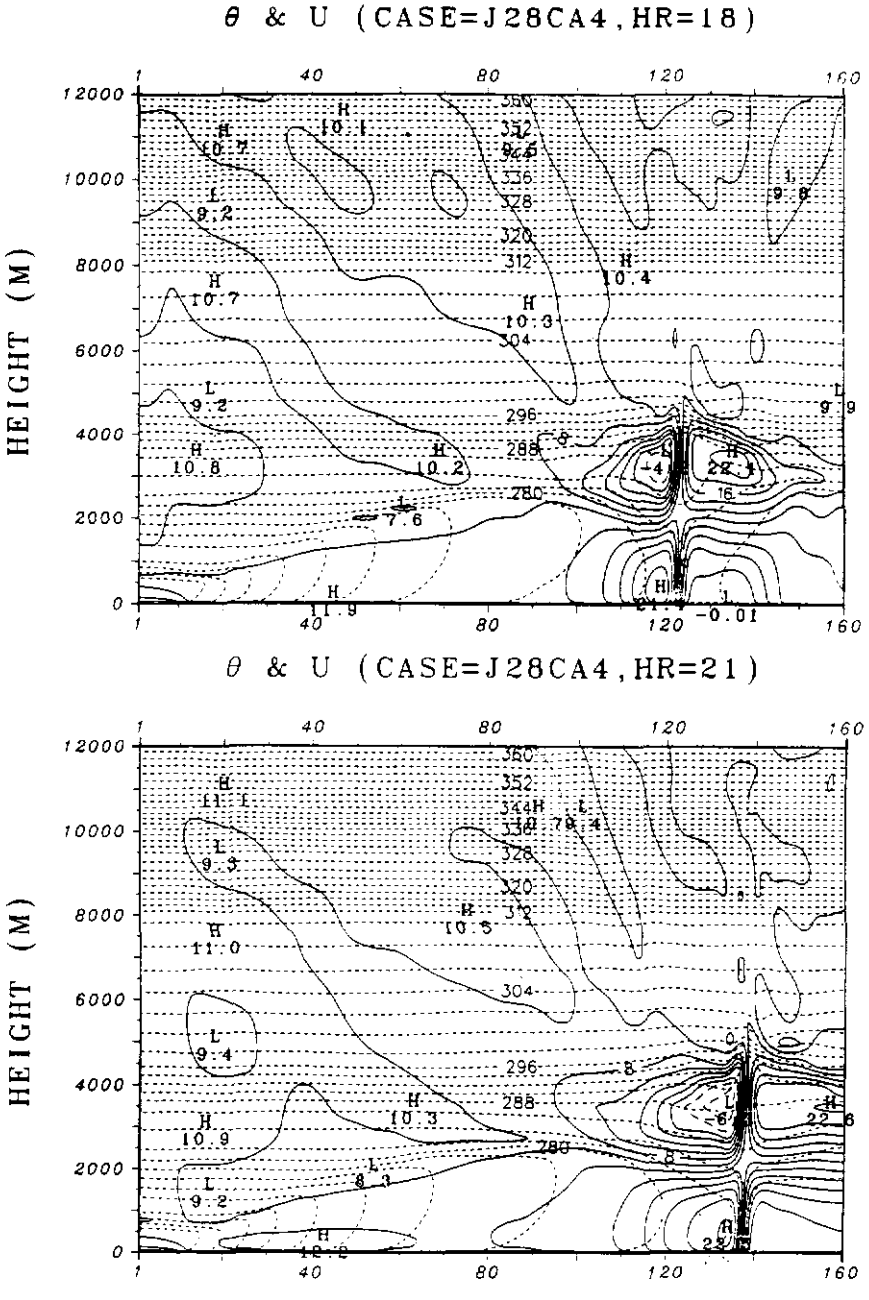

Fig. 16. The results for θ (shorter dashed lines) and u (longer dashed and solid) at 18 and 21 h for case J28CA4 (offshore barotropic flow with the tropopause). Contour intervals are 2°K for θ and 2 m s^{-1} for u.

for J28CA4 are similar to the ones for the case J28CA1, indicating that the development of the MBL updraft depends primarily on the low-level flow.

Density mountain waves at upper levels in baroclinic flow do not appear in barotropic flow, which is evident in Figure 16. Penetration of MBL-induced clouds in barotropic flow slightly lifts the strongly stratified u-shear layer without causing significant upper-level perturbation motions. Outward radiation of wave energies from convective clouds (around grid 122) is prominent, as indicated by the limb-type of vertical velocities. The waves generated in baroclinic flow can propagate more efficiently as compared to barotropic flow since the Scorer number for barotropic flow is much smaller because there is no contribution by shear. Hence, barotropic flow must satisfy the relationship $k_m < l$ for propagating mountain waves, where k_m is the wavelength of the density mountain. The barotropic waves are thus constrained to low levels, similar to evanescent mountain waves (Smith, 1979).

E. Response to onshore ambient flow

A previous study (Huang and Raman, 1990a) showed that the coastal and Gulf Stream rainbands could be produced by onshore flow if the inland air is considerably colder than the ocean water. A case (J28CD1) similar to J28CA1, but with reversed flow (onshore), was simulated. The simulated region over the land was also increased to include the Appalachians for this onshore flow condition. Figure 17 shows the results at 24 h for this case. As can be seen, the shallow coastal front below 2 km (see dashed lines near the coastline at grid 120) could be maintained even after 24 h of maritime air advection. There are widespread stratocumulus clouds (solid lines) over the entire inland region caused by the lifting effects of the mountains and the front. Because of the relatively dry initial conditions for this case, no rainband is produced over the land. The circulation at the frontal region also shows similar upper-level waves as found in the offshore flow except that the density mountain (near grid 122) slopes up to the east.

4. Discussions

A. Role of eddy Prandtl number

It was shown in Part I that the variation in the eddy Prandtl number does not cause a considerable change in the prediction of 1-D PBL flow. As the flow becomes multi-dimensional, the importance of the Prandtl number, however, could significantly increase because of advection effects. A question then immediately arises. Why does a turbulence closure with a constant P_{rt} (defined as K_θ/K_M, i.e., the inverse Prandtl number) of unity produce stronger updrafts and rainbands for both 2-D onshore and offshore flows, compared to the one using the level 2.5 formulation which normally gives a larger P_{rt} (about two) in the convective PBL flow? From Figure 14, the case J28CA2 (with $P_{rt} = 1$) appears to yield larger

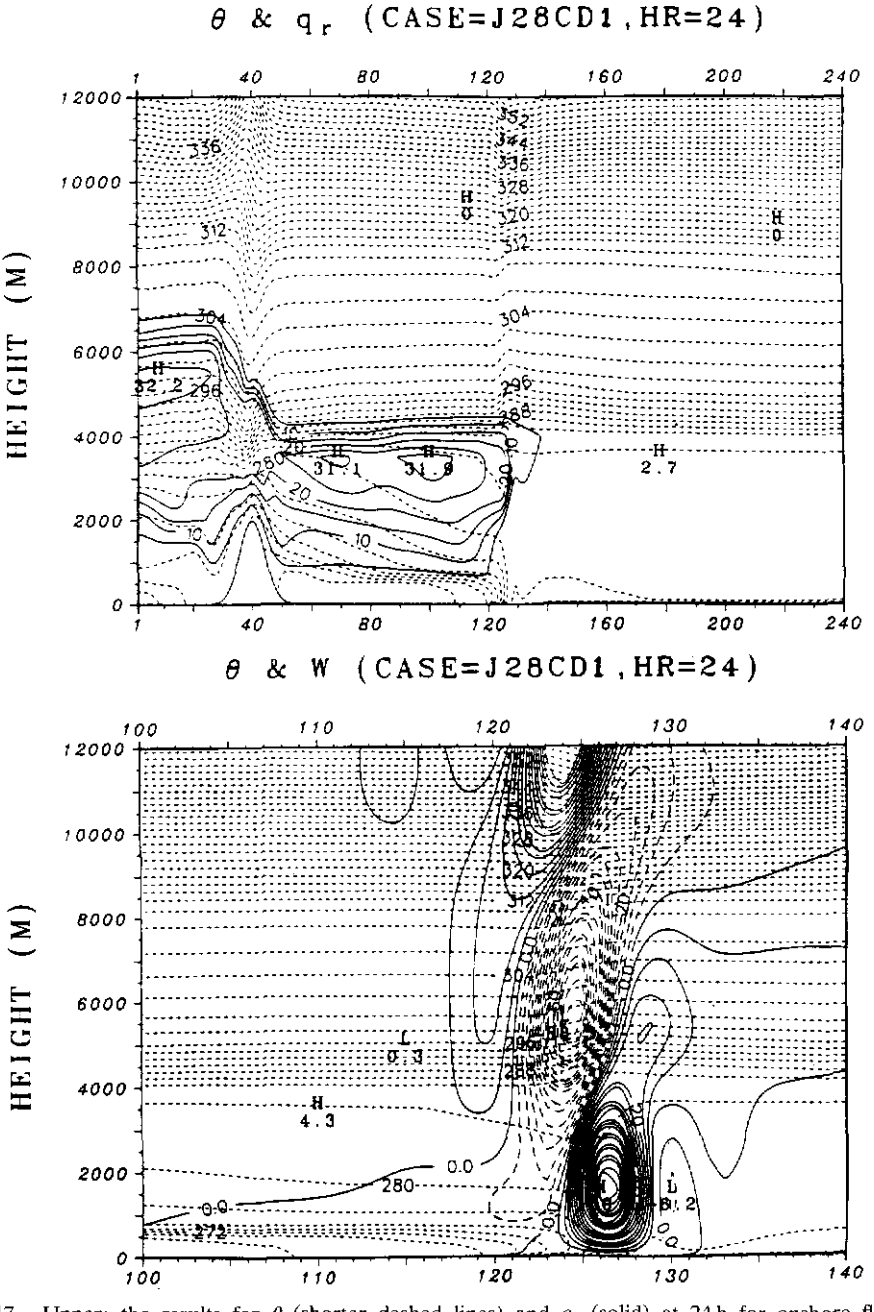

Fig. 17. Upper: the results for θ (shorter dashed lines) and q_c (solid) at 24 h for onshore flow (J28CD1); lower: the close-up of the circulation near the coastal region for w (longer dashed and solid). Contour intervals are 2°K for θ, 5 cm s^{-1} for w and 0.05 g kg^{-1} for q_c.

horizontal gradients of turbulent heat fluxes in the updrafts as compared to J28CA1, despite the fact that the latter in general has stronger turbulent heat fluxes in most of the MBL.

Both the 1-D and 2-D results show that the level 2.5 case appears to give larger eddy diffusivities and inverse Prandtl numbers in convective conditions. With smaller eddy diffusivities, the structure of the MBL for the case J28CA2 (with $P_{rt} = 1$) tilts more downstream, as compared to J28CA1 (with the level 2.5 formulation). As more clouds develop and begin to interact strongly with the underlying MBL, the tilting increases downstream even farther. Thus, the horizontal gradient of the thermal fields is a major factor responsible for the difference in the development of the MBL system. A larger ratio between K_θ and K_M (i.e., turbulent transfer is more efficient for heat than for momentum) leads to a reduction in the updraft intensity since the thermals are more upright. The slantwise convection tends to produce larger horizontal temperature gradients as compared to the upright convection (see Figures 7 and 9). Advection effects also increase in the more slantwise convection, producing a closer packing of isentropics. This aspect may also be associated with certain types of flow instabilities to be discussed later.

B. Effects of baroclinity

For barotropic flow, only upright convection is found at low levels (case J28CA4), in contrast to the density mountain waves triggered by the middle-level baroclinity in J28CA1. Clearly, the results indicate an important role of baroclinity in producing a regime of upward motion at levels above the MBL. It is possible that the density mountain waves could produce upper-level clouds as the airflow at these levels is not dry (see Figure 2). The configuration of the clouds east of the Gulf Stream for both barotropic and baroclinic offshore flows exhibits a single convergence zone, in contrast to the observed cloud streets as indicated by the satellite imagery (Wayland and Raman, 1989). These propagating cloud streets are probably related to lee waves triggered by a middle-level density mountain. The lee waves, however, cannot be simulated by our numerical model using the hydrostatic assumption.

C. Instability of the MBL updrafts

One of the interesting results in this study is the rapid development of the circulation system for all cases. As discussed before, the MBL updrafts begin to intensify in the presence of clouds. The rapid development of updrafts is thus mostly the result of conditional symmetric instability (CSI) in a moist environment, similar to that in dry flow (Hoskins, 1974). A brief review of CSI has been given by Knight and Hobbs (1988). The CSI theory indicates that for linear flow, a decrease (an increase) in the vertical (horizontal) gradient of equivalent potential temperature θ_e will result in a greater growth rate of perturbation motion (e.g., Bennetts and Hoskins, 1979). The CSI mechanism may also explain why stronger updrafts can be produced in the more slantwise convection discussed before.

Since strong middle-level atmospheric baroclinic flow (J28CA1) and barotropic flow (J28CA4) both show a similar development of the circulation system, the instability of the MBL updrafts must therefore be induced thermodynamically. Obviously, flow instability in this region must be initiated by the effects of SST gradients, according to the CSI theory. During the MBL modification, a horizontal gradient of air temperature is required for the presence of updrafts. At the initial stage of development, however, turbulent transfer in the convective MBL tends to dominate advection. Thus, the MBL resembles Benard convection with uniform heating. At the same time, there is a build-up of a local pressure gradient induced by differential heating. This leads to the formation of a baroclinic zone. The updrafts then develop and become stronger as clouds form locally. As the transport of larger θ_e exceeds the lifting condensation level of the flow, the clouds develop more quickly and facilitate a faster growth of the updrafts because of the decreased $\partial\theta_e/\partial z$ (favoring convective instability). Thus, the mechanism of CSI rather than convective instability best describes the development of low-level updrafts over the Gulf Stream region. The CSI mechanism has also been applied to cold frontal rainbands (Knight and Hobbs, 1988). Applicability of the CSI theory in the development of the MBL system was investigated further in the 3-D simulation of the Gulf Stream rainbands (Huang, 1990; Huang and Raman, 1990b).

D. Nonhydrostatics

Finally, nonhydrostatic influences on the flow should be discussed since the 5 km horizontal resolution used in this study is probably close to the limiting scale of the hydrostatic assumption for mesoscale circulations over the Gulf Stream region. Pielke (1984) discussed in detail the appropriateness of using a hydrostatic model to simulate sea breeze circulations, and concluded that nonhydrostatic effects are negligible even for a breeze convergence zone of less than 6 km. From Figures 3 and 7, the relative importance of nonhydrostatic effects on MBL updrafts may be roughly estimated by the following scale analyses:

$$\partial w/\partial t = 1\ \mathrm{m\,s^{-1}}/3600\ \mathrm{s} = \mathrm{O}(10^{-3}),$$

$$u\partial w/\partial x = 30\ \mathrm{m\,s^{-1}} \times 1\ \mathrm{m\,s^{-1}}/30000\ \mathrm{m} = \mathrm{O}(10^{-3}),$$

$$w\partial w/\partial z = 1\ \mathrm{m\,s^{-1}} \times 1\ \mathrm{m\,s^{-1}}/1000\ \mathrm{m} = \mathrm{O}(10^{-3}),$$

$$\partial(K_M \partial w/\partial z)/\partial z = 300\ \mathrm{m^2\,s^{-1}} \times 1\ \mathrm{m\,s^{-1}}/10^6\ \mathrm{m^2} = \mathrm{O}(10^{-3}),$$

$$\rho'/\rho g = (\rho - [\rho])/\rho \times 9.8\ \mathrm{m\,s^{-2}} = \mathrm{O}(10^{-1}) \text{ for 1\% density variation.}$$

In the above, $[\rho]$ is the average air density over the oceanic region. Here, ρ' can not be easily determined since the initial air density has been modified everywhere over the ocean. Scale analysis for the turbulent transfer of vertical velocity would be more difficult if maximum magnitudes of the eddy diffusivity and the vertical velocity do not have a simple correlation. Therefore, vertical variations of the above terms were estimated over the region of maximum oceanic updraft at 18 h for the case J28CA1. The effect of density variation was found to be of the order

of 10^{-1} m s^{-2} for $g\rho'/\rho$ or 10^{-2} m s^{-2} for $g(\partial\rho/\partial x\Delta x)/\rho$ in the updrafts. The turbulent transfer is of the order of 10^{-3} m s^{-2} near the surface but only 10^{-5} m s^{-2} in the region of maximum updrafts. Vertical advection in this region is of the order of 10^{-3} m s^{-2} and is larger than horizontal advection which is of the order of 10^{-4} m s^{-2}. Above the MBL, however, horizontal advection (of the order of 10^{-3} m s^{-2}) is more important than vertical advection since the baroclinic flow is stronger at upper levels. In this study, the resolved scale is about 30 km for updrafts. Hence, nonhydrostatic processes do not seem to play an important role in this transient system.

5. Conclusions

A two-dimensional (2-D) mesoscale numerical model is used to simulate a January 28 cold-air outbreak over the Gulf Stream region during GALE IOP-2 (1986). The model utilizes a turbulence closure which involves turbulent kinetic energy (TKE) and dissipation (ϵ) equations and combines the level 2.5 formulation of Mellor and Yamada (1982) to determine eddy Prandtl number.

Using the E-ϵ turbulence closure, the modeled MBL is in good agreement with observations (Wayland and Raman, 1989), showing a low-level jet west of the warm core of the Gulf Stream and a constrained boundary-layer height due to the middle-level (2–4.5 km) stable layer. The MBL induced single cloud and rain band first appears east of the Gulf Stream; this band then moves offshore at the same speed as the circulation front. This front is similar to typical sea breeze penetrative fronts, and it moves at a slightly slower speed than the ambient flow. The results also indicate that removal of the tropopause does not influence the low-level circulation and the movement of the front. The speed of the front is slightly greater in baroclinic downshear flow than in barotropic flow. The general structure of the low-level circulation, however, depends primarily on low-level wind speed rather than middle-level baroclinity. Our results also imply that the high-cloud streets observed downwind of the Gulf Stream are possibly related to upper-level baroclinic lee waves, which are triggered by an elevated density mountain. The density mountain waves, however, become evanescent as the baroclinity (which gives a larger Scorer parameter) is removed. The results are in agreement with mountain wave theory (Smith, 1979).

The modeled 2-D MBL circulation is found to be sensitive to variations in eddy Prandtl numbers, in contrast to the 1-D model results discussed in Part I. The MBL circulation becomes even more sensitive to the eddy Prandtl number as the clouds begin to interact with the MBL. A constant inverse eddy Prandtl number of unity produces more intense slantwise convection compared to the upright convection simulated by the level 2.5 case with larger inverse eddy Prandtl numbers. Cloud development is stronger in slantwise than in upright convection. Slantwise convection tends to produce larger horizontal temperature gradients as compared to upright convection. The level 2.5 formulation gives a more reasonable

entrainment depth probably because this turbulence closure determines the eddy Prandtl number with better physics. It appears that the fast development of clouds is caused by conditional symmetric instability (CSI) which begins after MBL baroclinity reaches a critical magnitude. The onset of the CSI begins at about the time that the height of the MBL exceeds the lifting condensation level (LCL). Variations in the magnitude of slantwise convection do not influence the height and geometry of the cloud and rain bands, but can produce differences in their intensity. The CSI mechanism in the MBL circulation was examined in greater detail in the 3-D simulation of the Gulf Stream rainbands (Huang and Raman, 1990b).

Acknowledgements

The authors wish to thank Dr. G. S. Janowitz or several helpful discussions. This study was supported by the Division of Atmospheric Sciences, National Science Foundation under grants ATM-83–11812 and ATM-88–01650.

References

Bennetts, D. A. and Hoskins, B. J.: 1979, 'Conditional Symmetric Instability–a Possible Explanation for Frontal Rainbands', *Q. J. R. Meteorol. Soc.* **105**, 945–962.

Dirks, R., Kuettner, J. P., and Moore, J.: 1988, 'Genesis of Atlantic Lows Experiment (GALE): An Overview', *Bull. Amer. Meteorol. Soc.* **69**, 148–160.

Knight, D. and Hobbs, P. V.: 1988, 'The Mesoscale and Microscale Structure and Organization of Clouds and Precipitation in Midlatitude Cyclones. Part XV: A Numerical Modeling Study of Frontogenesis and Cold-Frontal Rainbands', *J. Atmos. Sci.* **45**, 915–928.

Hoskins, B. J.: 1974, 'The Role of Potential Vorticity in Symmetric Stability and Instability', *Q. J. R. Meteorol. Soc.* **100**, 480–482.

Huang, C. Y.: 1990, 'A Mesoscale Planetary Boundary Layer Numerical Model for Simulations of Topographically Induced Circulations', Ph.D. dissertation submitted to the Department of Marine, Earth and Atmospheric Sciences, North Carolina State University, Raleigh, 253 pp.

Huang, C. Y. and Raman, S.: 1988, 'A Numerical Modeling Study of the Marine Boundary Layer Over the Gulf Stream during Cold Air Advection', *Boundary-Layer Meteorol.* **45**, 251–290.

Huang, C. Y. and Raman, S.: 1990a, 'Numerical Simulations of Cold Air Advection over the Appalachian Mountains and the Gulf Stream', *Mon. Wea. Rev.* **118**, 343–362.

Huang, C. Y. and Raman, S.: 1990b, 'A Three-Dimensional Numerical Investigation of Carolina Coastal Front and the Gulf Stream Rainband', submitted to *J. Atmos. Sci.*

Huang, C. Y. and Raman, S.: 1991, 'Numerical Simulation of Jan. 28 Cold Air Outbreak During "GALE" I, The Model and Sensitivity Tests of Turbulence Closures', *Boundary-Layer Meteorol.* **55**, 381–407.

Mellor, G. L. and Yamada, T.: 1974, 'A Hierarchy of Turbulence Closure Models for Planetary Boundary Layers', *J. Atmos. Sci.* **31**, 1791–1806.

Mellor, G. L. and Yamada, T.: 1982, 'Development of a Turbulence Closure Model for Geophysical Fluid Problems', *Rev. Geophys. Space Phys.* **20**, 851–875.

Mailhot, J. and Benoit, R.: 1982, 'A Finite Element Model of the Atmospheric Boundary Layer Suitable for Use with Numerical Weather Prediction Models', *J. Atmos. Sci.* **39**, 2249–2266.

Miller, J. E.: 1946, 'Cyclogenesis in the Atlantic Coastal Region of the United States', *J. Meteorol.* **3**, 31–44.

Pielke, R. A.: 1984, *Mesoscale Meteorological Modeling*, Academic Press, New York, 612 pp.

Raman, S. and Riordan, A. J.: 1988, 'The Genesis of Atlantic Lows Experiment (GALE): The Planetary Boundary Layer Subprogram', *Bull. Amer. Meteorol. Soc.* **69**, 161–172.

Smith, R. B.: 1979, 'The Influence of Mountains on the Atmosphere', *Adv. Geophys.* **21**, 87–230.

Sun, W.-Y. and Ogura, Y.: 1980, 'Modeling the Evolution of the Convective Planetary Boundary Layer', *J. Atmos. Sci.* **37**, 1558–1572.

Yamada, T. and Mellor, G.: 1975, 'A Simulation of Wangara Atmospheric Boundary Layer Data', *J. Atmos. Sci.* **12**, 2309–2329.

Wayland, R. and Raman, S.: 1989, 'Mean and Turbulent Structure of a Baroclinic Marine Boundary Layer during the 28 January 1986 Cold-Air Outbreak (GALE86)', *Boundary-Layer Meteorol.* **48**, 227–254.

Uccellini, L. W., Brill, K. F., Petersen, R. A., Keyser, D., Aune, R., Kocin, P. J. and des Jardins, M.: 1986, 'A Report on the Upper Level Wind Conditions Preceding and During the Shuttle Challenger (STS 51L) Explosion', *Bull. Amer. Meteorol. Soc.* **67**, 1248–1265.